

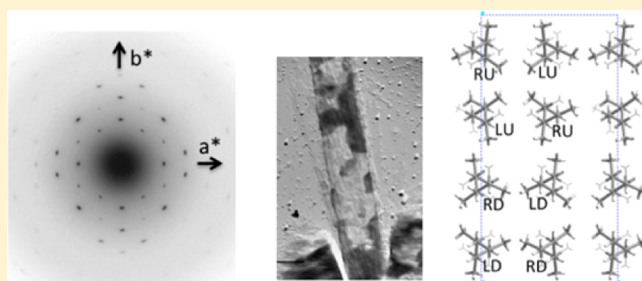
## A New $\epsilon$ Crystal Modification Found in Stereodefective Isotactic Polypropylene Samples

Bernard Lotz\*

Institut Charles Sadron, CNRS, and Université de Strasbourg, 23 rue du Loess, B.P. 84047, 67034 Strasbourg, Cedex, France

 Supporting Information

**ABSTRACT:** The main features of an original crystal modification of isotactic polypropylene (iPP) are described. This form is obtained with a stereodefective or “an-isotactic” iPP produced with a zirconocene catalyst by Rieger et al. [Macromolecules 1990, 23, 3559–3568]. In thin films, most of the material crystallizes as composite crystals made of  $\alpha$  phase backbones with large amounts of  $\gamma$  phase overgrowths. The new form is nucleated by a crystal–crystal growth transition on parent  $\alpha$  phase crystals. It is probably produced with only the most stereodefective part of the material. The single crystals formed in thin films are very similar to the  $\alpha$ iPP elongated laths but do not display any of their overgrowths ( $\alpha$ – $\alpha$  lamellar branching or  $\alpha$ – $\gamma$  epitaxial relationship). The electron diffraction evidence ( $hk0$  and  $hk1$  reflections accessed from flat-on and tilted single crystals, respectively) indicates an orthorhombic unit cell with parameters  $a = 12.50 \text{ \AA}$ ,  $b = 24.60 \text{ \AA}$ , and  $c = 6.5 \text{ \AA}$  that houses eight stems (space group  $Pccn$ ). The chain conformation is the archetypical  $3_1$  helix of the  $\alpha$ ,  $\beta$ , and  $\gamma$  forms of iPP but arranged in a near-double-tetragonal packing. As in  $\alpha$ iPP, four distinct layers are packed along the  $b$ -axis (that is however  $\approx 4 \text{ \AA}$  longer), but the  $a$ -axis repeat distance is nearly doubled. Stereodefects ( $rr$  defects in all  $m$  sequences) induce “abnormal” locations of the methyl groups as exist in polyisobutylene. These defects generate a near-irrational helix projection that translates in an unusual tetragonal-like packing (for 3-fold helices) and results in a low-density metastable crystal structure.



### INTRODUCTION

Isotactic polypropylene (iPP) is famous for its crystal polymorphism and highly original packing modes that, strikingly, rest on the same 3-fold helix conformation.<sup>1</sup> In the  $\alpha$  phase ( $\alpha$ iPP), four different layers are packed along the  $b$ -axis. They differ by the helix chirality, up–down orientation (clinality), and azimuthal setting.<sup>2</sup> Occasionally, a stacking mistake brings two layers made of isochiral helices in contact with the helix axes  $80^\circ$  apart (through the agency of an epitaxial registry or a rotation twin), which induces a lamellar branching—the only well-documented example of this type in polymer crystallography.<sup>3</sup> In the  $\gamma$  phase ( $\gamma$ iPP), this stacking mistake becomes a crystallographic feature and generates a structure with nonparallel chain axes—again a singularity in polymer crystallography.<sup>4</sup> The  $\beta$  phase ( $\beta$ iPP) is a trigonal, frustrated structure made of isochiral helices.<sup>5</sup> More recently, polymers of propene with more than  $\approx 10\%$  hexene or pentene comonomers were shown to maintain the 3-fold helical symmetry, but owing to the presence of a fraction of monomers with longer side chains, the helices pack in the trigonal unit-cell characteristic of Form I of isotactic poly(1-butene) (iPBu) with space group  $R\bar{3}c$  or  $R\bar{3}c$ . This crystal structure, christened  $\delta$ iPP, is not therefore characteristic of iPP as such but indicates that iPP finds original structural responses to accommodate what amounts to chemical “defects” of the chain.<sup>6</sup>

The present report describes a novel and elusive crystal structure of stereodefective isotactic polypropylene produced with a zirconium-based catalyst. This specific material, synthesized and investigated by Rieger et al., crystallizes mostly in the  $\gamma$  crystal modification.<sup>7</sup> In the present investigation, only a limited number of single crystals of the new modification have been observed in thin film growth. This modification shares several structural features with  $\alpha$ iPP. In particular, it has a similar sequence of four layers along the  $b$ -axis. The  $a$ -axis is however doubled, and the 3-fold helices pack in a nearly tetragonal fashion—a definite oxymoron. The unusual characteristics of this new phase of iPP, chronologically named the  $\epsilon$  phase ( $\epsilon$ iPP), illustrate the conformational and packing adaptations of iPP to the presence of stereodefects.<sup>8</sup>

### EXPERIMENTAL SECTION

**Materials.** The sample was kindly provided by Pr. J. C. W. Chien (University of Massachusetts, Amherst). It is part of an extensive study by Rieger et al.<sup>7</sup> on the influence of the catalysts on the stereochemical control (or tacticity) of polypropylene. These materials were described as “an-isotactic” polypropylenes, a terminology that has been superseded by “stereodefective” in the literature. The authors indicate that the “polypropylenes have been obtained with a racemic ethylene-

**Received:** May 13, 2014

**Revised:** October 5, 2014

**Published:** October 31, 2014

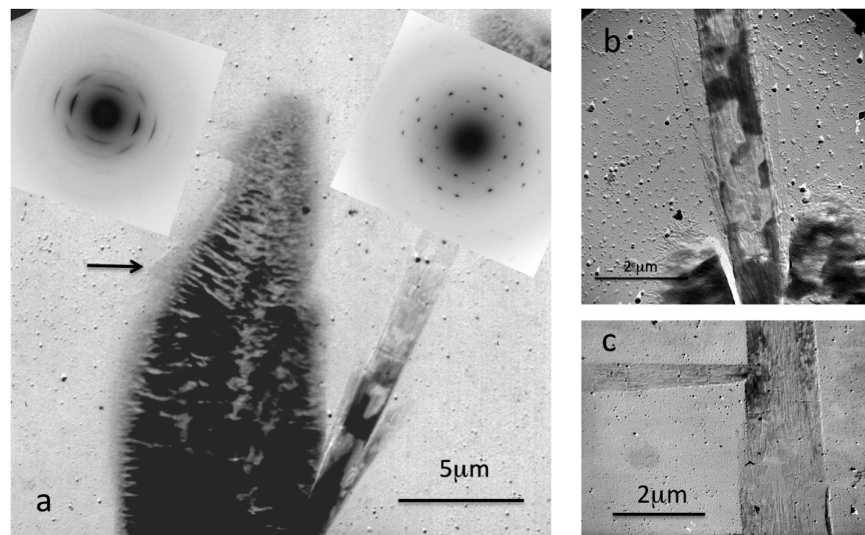


**Figure 1.** Morphology of thin film grown stereodefective iPP single crystals. (a) Left: a lenticular, mixed  $\alpha/\gamma$  crystal as assessed by its diffraction pattern and morphology. The  $\alpha$  lamella is the spine of the composite crystal. Edge-on overgrowth of  $\gamma$  crystals generates the dark horizontal stripes. The tip of a flat-on, toppled-over  $\gamma$  crystal is arrowed (cf. also Figure S1 for the structural model). Right: lamella of  $\epsilon$ iPP as assessed from its diffraction pattern. (b)  $\epsilon$ iPP lamella nucleated at the tip of an  $\alpha/\gamma$  composite crystal. (c) Growth twin of  $\epsilon$ iPP. Note the right angle orientation of the daughter lamella and the absence of overgrowths as exist in composite  $\alpha/\gamma$  crystals.

bis(indenyl)-zirconium dichloride/methyl aluminoxane (MAO) catalyst from  $-55$  to  $+80$   $^{\circ}\text{C}$  and Al/Zr ratios between  $10^3$  and  $1.6 \times 10^4$ . As the polymerization temperature increases, the polymers produced have progressively lower melting transition temperature, lower homosteric pentad sequence population, and higher solubility in low-boiling solvents, indicating frequent stereochemical inversion in monomer enchainment. Polymer fractions separated by solvent extraction are relatively crystalline (crystallinity  $>50\%$ ) favoring a thermally stable  $\gamma$  modification<sup>7</sup>. The sample used in these studies is one of those fractions that crystallize “mostly in the  $\gamma$  modification”. Unfortunately, both the details of the material and the material itself were lost when our laboratory moved to its new location. These circumstances are quite unfortunate, but they do not weaken the major message conveyed by this work—observation of a new crystal modification of stereodefective iPP. In addition, the new phase is only a very minor component of the material produced during the (slow) crystallization process. Future studies will help precise the range of concentrations of defects that are most likely to induce this crystal phase.

**Preparation and Investigation Techniques.** Since only a limited amount of material was available, well-established preparation techniques adapted for electron microscopy examination are mandatory. The single crystals are produced from thin polymer films cast on a mica or glass cover slide from a 0.5% solution in *p*-xylene. The films are melted at 180  $^{\circ}\text{C}$  in a Mettler FP80 heating stage under nitrogen atmosphere and slowly ( $0.1$   $^{\circ}\text{C}/\text{min}$ ) cooled through the crystallization range and down to  $\approx 40$   $^{\circ}\text{C}$ . The sample is backed with a carbon film and examined in an optical microscope in order to select the areas of interest. These areas only are stripped off the glass or mica support with the help of a poly(acrylic acid) backing. The films are collected on copper grids and examined with a Philips CM12 electron microscope equipped with a rotation/tilt stage ( $\pm 60^\circ$ ). The diffraction patterns are collected on Agfapan and/or on plain daylight films. The daylight films saturate rather rapidly, which helps enhance the critical, frequently tale-telling weaker reflections of the diffraction pattern (down to  $1.55 \text{ \AA}^{-1}$  in the present case; cf. Figure 2a). This procedure has also limitations. The intensities recorded cannot be analyzed quantitatively, although a qualitative comparison of intensities remains possible. The  $hk0$  diffraction patterns are calibrated with TlCl vapors. In patterns of tilted crystals, the relevant  $h00$  or  $0k0$  reflections are used as internal standards.

**Modeling and Analysis of the Data.** Molecular modeling of the structures and calculation of the diffraction patterns are performed on

a Silicon Graphics Octane workstation, using the various modules available in the Cerius<sup>2</sup> package developed by Accelrys (San Diego, CA, and Cambridge, UK).<sup>9</sup> Minimization of the packing energy is performed with the “Crystal Packer” and “Minimizer” modules. The “Crystal Packer” module turns out to be most useful in polymer science, since it maintains the chain axis of the polymer parallel to the crystallographic *c*-axis, a feature that is not included in the “Minimizer” module. The potentials most frequently used are “Universal 1.02”. The analysis concentrates on the possible and plausible packing schemes that would be consistent with the available diffraction evidence. Given the limitations of the diffraction intensity data and the uncertainties associated with the random location of the stereodefects, the present models should be considered first-order approximations. More detailed models will become available when using the newly developed precession methods in electron diffraction<sup>10</sup> or if and when a relatively “pure” sample of this new crystal phase of iPP can be obtained in a fiber form suitable for conventional X-ray fiber analysis.

## RESULTS

### Single Crystals: Morphology and Unit-Cell Geometry.

**Single Crystals Morphology.** The thin films of stereodefective iPP crystallized by slow cooling to room temperature display two populations of crystals. The first population consists of classical “quadrites” of iPP. They correspond to edge-on growth of crystals with the  $\alpha$ iPP *ac* face parallel to the substrate (Figure S1). In the present case, the branches of the quadrites are highly bent, which is a characteristic morphological trademark: it indicates that  $\alpha$ iPP and  $\gamma$ iPP coexist in these quadrites.<sup>11</sup> The second population consists of elongated, sometimes slightly lenticular crystals. They are composite crystals made of a flat-on  $\alpha$ iPP “backbone” crystal that serves as a substrate for  $\gamma$ iPP overgrowth. The latter crystals are tilted at  $\approx 40^\circ$  to the substrate and  $\alpha$ iPP laths, thus the appearance of thicker, roof tiles overgrowths (Figure 1a, left). Occasionally also, these  $\gamma$ iPP crystals “fall” on the substrate glass slide and produce triangular overgrowths with their fastest *c*-axis growth direction oriented at right angles to the  $\alpha$ iPP major growth direction (arrowed in Figure 1a). The nature of these composite  $\alpha/\gamma$ iPP crystalline entities is confirmed by electron diffraction (left inset of Figure 1a). Their structure has been analyzed in full detail in an earlier

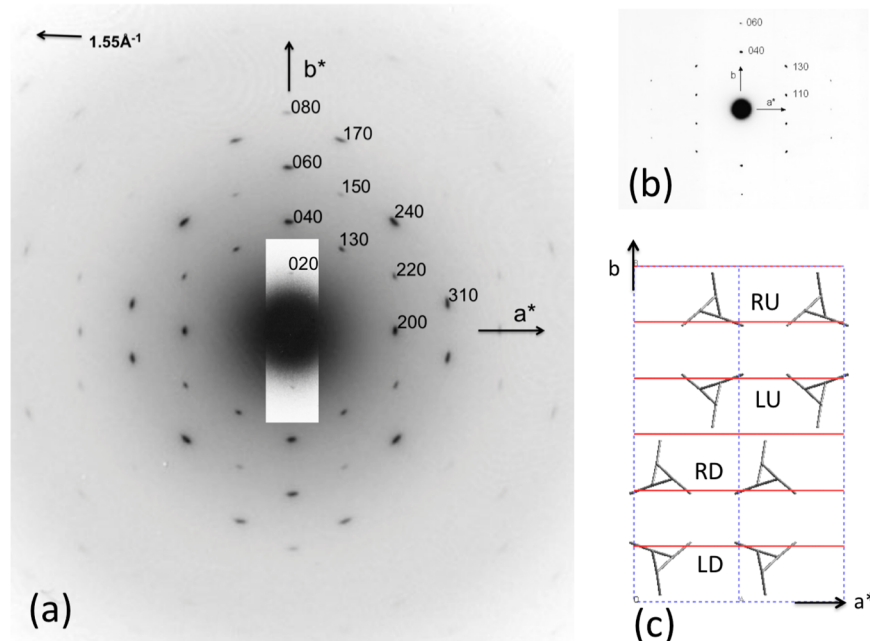


**Figure 2.** (a)  $hk0$  selected area electron diffraction pattern of an  $\epsilon$ iPP single crystal. Indexing based on an orthorhombic unit-cell with parameters  $a = 12.5 \text{ \AA}$  and  $b = 24.6 \text{ \AA}$ . Note the presence of a weak 020, of 040 and 060 reflections. (b) For comparison purposes, selected area electron diffraction pattern of an  $\alpha_2$ iPP single crystal displaying the presence of the critical 060 reflection. (c) Two unit cells of the structure of  $\alpha_2$ iPP. Monoclinic unit cell with  $a = 6.65 \text{ \AA}$ ,  $b = 20.96 \text{ \AA}$ ,  $c = 6.5 \text{ \AA}$ ,  $\beta = 99.20^\circ$ , and space group  $P2_1/b$ . The helical hand (right or left) and clinicity (up or down) of layers along the  $b$ -axis is indicated. The 060 periodicity is highlighted.

work that helped confirm the nonparallelism of the chains in  $\gamma$ iPP (Figure S2).<sup>12</sup> The bent quadrates and the composite crystals represent by very far the major components of the material.

Strikingly, however, some of the flat-on crystals do not fit in this pattern. These crystals are frequently generated on the lateral edges (Figure 1a) or the tip (Figure 1b) of the  $\alpha/\gamma$ iPP composite crystals. They are elongated laths, i.e., very similar to the “conventional”  $\alpha$ iPP laths. These crystals are however of a different nature, since they *do not* induce the growth or overgrowth of “daughter” crystals, either of the  $\alpha$  or  $\gamma$  phase. In Figure 1b, the new crystal was apparently nucleated in the middle of the parent end growth edge. The different crystal has a significantly larger growth rate than the  $\alpha$ iPP crystals. Because of its higher growth rate, the crystal of the new species feeds on the available molten material in the thin film ahead of the  $\alpha$  phase laths, thus the “flat” tip of these  $\alpha$  phase laths (and  $\gamma$  phase overgrowths). Finally, Figure 1c illustrates a growth twin of this different crystal type. The branch grows at right angle to the parent crystal. This branch does not however result from the conventional  $\alpha$ iPP lamellar branching giving rise to quadrates.  $\alpha$ iPP lamellar branching results from a rotation twin on the lateral  $ac$  faces of the laths. The branched lamella would thus grow *out of the plane* of the preparation (cf. Figure S2). In the present case by contrast, the parent and daughter lamellae are *coplanar* and the chain axes are *parallel*. This branch is induced by a conventional  $hk0$  growth twin—specifically, and anticipating the later crystal structure analysis, a 120° growth twin.

The morphologies shown in Figure 1 suggest that the different crystal form has a specific orientation relationship with the “parent”  $\alpha$  phase crystals. The long axis of these crystals is nearly parallel to the long axis of the parent  $\alpha$ iPP laths. From the experimental evidence available (only a limited number of

such crystals have been observed), this relationship is frequent, and even possibly systematic. The filiation appears to result from a possible crystal–crystal growth transition, at least under the present growth conditions. Also, this nucleation takes place relatively late in the crystallization process, apparently after a significant amount of the available material has already crystallized in the combined  $\alpha/\gamma$ iPP entities. However, once nucleated, the (remaining?) molten material crystallizes in this different form. These observations provide contradictory messages as to a possible selection of molecular stereoregularity during crystallization. Late nucleation would suggest that only the most stereodefective part of the material may crystallize in this different form, but *the same molecules appear to become part of any one of the known forms of iPP:  $\alpha$  or  $\gamma$  or now also  $\epsilon$  iPP phase* (when available), depending on the local nucleation and/or crystallization conditions. The impact of the molecular features should be analyzed in more detail in future work. At any rate, the new crystal form seems to also fit in this pattern.

**Single Crystals: Diffraction Data.** The single crystals display a highly original diffraction pattern that has no equivalent for isotactic polypropylene or for any other polyolefin (Figure 2, indexing based on the structural model developed next). Its orthogonal symmetry indicates either an orthorhombic unit cell or possibly a monoclinic cell as seen in  $c$ -axis projection—the latter situation being very reminiscent of  $\alpha$ iPP (Figure 2b). The spacings of the most intense, inner reflections in Figure 2a are around 6 Å (actually, 6.25 and 6.15 Å). The many weaker reflections in this diffraction pattern indicate an unconventionally large unit cell with parameters  $a = 12.5 \text{ \AA}$  and  $b = 24.6 \text{ \AA}$ .

Tilting the single crystals around the  $a$ - and  $b$ -axes helps reach  $hkl$  reflections and thus provides information on the  $c$ -axis repeat distance. The diffraction patterns recorded from single crystals tilted around both  $a$ - and  $b$ -axes are displayed in Figure 3a,b. In both cases, the tilt angle is about 40°. No other tilt

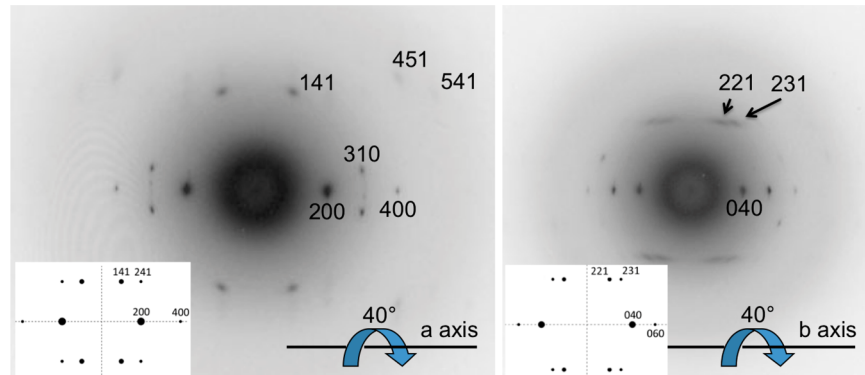


**Figure 3.** Electron diffraction patterns obtained after tilting the  $\epsilon$ iPP single crystal by  $40^\circ$  around the  $a$ -axis (left) and  $b$ -axis (right). The insets display the corresponding calculated diffraction patterns for  $42^\circ$  ( $a$ -axis) and  $43^\circ$  ( $b$ -axis) tilts using the structural model illustrated in Figure 5a. Note also the absence of any  $h01$  or  $0k1$  reflections on the “meridian” of these diffraction patterns.

angle (within the  $\pm 60^\circ$  range allowed by the tilting stage) yields any diffraction of significant intensity. Three major reflections only are observed on the first layer, although some weaker reflections can be seen in Figure 3a. They indicate a  $c$ -axis repeat distance of  $6.5 \text{ \AA}$ , assuming orthorhombic unit-cell geometry.<sup>13</sup> The calculated and measured spacings of the observed  $hkl$  reflections are collected in the Supporting Information (Table S5a).

To sum up the diffraction evidence, the new phase has most probably an orthorhombic cell geometry with cell parameters  $a=12.5 \text{ \AA}$ ,  $b=24.6 \text{ \AA}$ , and  $c=6.5 \text{ \AA}$ . Only  $hk0$  reflections with  $h+k$  even are observed. Even though the number of nonequatorial reflections is limited, the presence of both 221 and 231 indicates that no extinction conditions apply for  $hkl$  reflections. Another systematic absence is suggested for  $h01$  and  $0k1$  reflections: they are not observed.

**Derivation of the Crystal Structure. Guidelines in the Structure Derivation.** The morphology and diffraction data provide significant, but at the same time limited, guidelines in the derivation of the structure. This derivation rests therefore on extensive model building and comparison with the available diffraction information. At the same time, the model building is guided and to some extent even confined by a considerable body of structural information gathered on isotactic polyolefins. Let us briefly recall these most relevant elements at the onset.

(a) The orthogonal symmetry of the diffraction pattern with  $b \approx 2a$  suggests a nearly square packing scheme reminiscent of the tetragonal unit cells known for higher members of the polyolefin family with a more complex, “noncrystallographic” helical symmetry ( $7_2$  helix of isotactic poly(4-methyl-pentene 1) (P4MP1) in its Form I<sup>14</sup> or  $11_3$  helix of isotactic poly(1-butene) (iPBu), Form II<sup>15</sup>). Such a “square” packing scheme has never been observed for iPP. As such, it departs significantly from the packing scheme observed in  $\alpha$ iPP, in which successive bilayers along the  $b$ -axis are shifted by half an  $a$ -axis repeat distance and the 3-fold helices interdigitate when “lone” methyl groups face each other (Figure 1c).

(b) At the same time, an exactly opposite conclusion may be reached: the  $\alpha$ iPP and the new iPP structures must have related features. Strikingly, the  $\epsilon$ iPP  $0k0$  reflections parallel some characteristic features of  $\alpha$ iPP: very weak  $020$ , presence of both  $040$  and  $080$  but also presence of the  $060$  reflection. These similarities indicate that the crystal structure shares the four layers organization of  $\alpha$ iPP along the  $b$ -axis. Such a four-layer

structure was so far specific to  $\alpha$ iPP among all known structures of polyolefins (Figure 2b,c).

(c) The structure departs from  $\alpha$ iPP in one other important aspect. In the  $\alpha$ iPP structure, the  $a$ -axis periodicity corresponds to the distance between neighbor stems (Figure 2c). Here, it is doubled, which implies that two stems with different chain axis projections and/or azimuthal settings alternate along the  $a$ -axis. This doubling is an essential feature in the derivation of the structure and therefore needs to be developed in some detail.

Helices of isotactic polyolefins are defined by their helix chirality (right- or left-handed spiraling, R or L) and, in a crystal lattice, by the relative orientation of stems or clinicity (characterized by a conformational feature, namely the orientation of the C–C $\alpha$  bond vector projected on the helix axis: up versus down, U versus D). Helices that differ either by their chirality (R versus L) or orientation (U versus D) have different chain axis projections. By contrast, helices that differ by both chirality and orientation (RU and LD) have identical chain axis projections, since they are linked by mirror symmetry normal to the helix axis. Also, statistical structures with RU and RD or LU and LD orientations at each stem site have identical projections. These differences are relevant for iPP. The  $\alpha_1$ iPP form produced at low  $T_c$  is a statistical form with higher symmetry ( $C2c$ ) in which each stem site is occupied by either an up- or a down-pointing stem of a given helical hand. At fast growth rates, selection of the stems chirality is operative, but selection of the stem orientation (clinicity) is not. This is sterically reasonable, since up- and down-pointing isochiral helices are nearly isomorphous: the outside methyl groups mostly (but not uniquely) involved in interhelix interactions occupy similar crystallographic positions. For the  $\alpha_2$ iPP phase produced at high  $T_c$ s and slow growth rates, the selection process differentiates both the chirality (L/R) and the clinicity (U/D), thus the RU, LD, RD, and LU sequence of layers along the  $b$ -axis (space group  $P2_1/b$ ) illustrated in Figure 2c (intermediate situations have been described). Note however that the repeat distance along  $a$  corresponds to a single stem for both  $\alpha_1$ iPP and  $\alpha_2$ iPP crystal structures.

Another feature affects the chirality and clinicity of stems in the crystal structure of polyolefins. In an elegant analysis developed in the 1980s by Petraccone et al.<sup>16</sup> and by Sadler et al.,<sup>17</sup> the stereochemistry of isotactic polyolefins was shown to set constraints on the fold structure, which in turn sets constraints on the clinicity and/or chirality of the stems linked by folds. The argument is rather involved and will not be

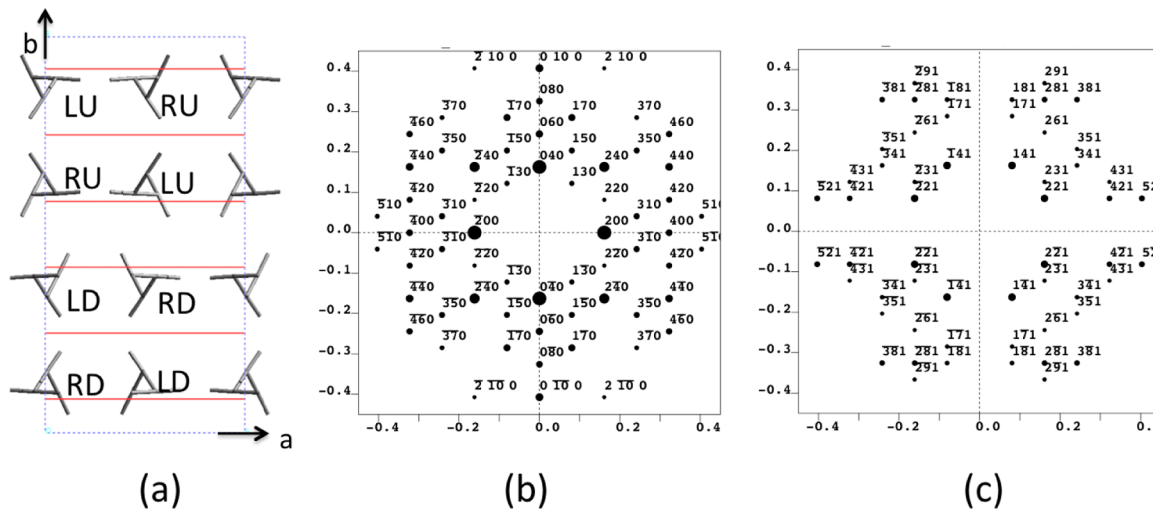


**Figure 4.** (a) Crystal structure of a “model” iPP in which the stereodefective methyl side chains of the 3-fold helices are not taken into account. Orthorhombic cell of the stereodefective material with dimensions  $a = 12.5 \text{ \AA}$ ,  $b = 24.6 \text{ \AA}$ , and  $c = 6.5 \text{ \AA}$ . The space group illustrated here is  $Pccn$ . Clusters of four “down” and four “up” helices alternate along the  $b$ -axis. Each cluster is made of two right-handed and two left-handed helices. The 060 periodicity has been underlined. (b) Calculated  $hk0$  diffraction pattern captures the essential features of the experimental pattern (Figure 2a). Note that several different cell symmetries and thus organizations of stems (helical hand and up/down orientations) yield the same  $hk0$  diffraction pattern. Some of these possibilities are shown in Figure S4. (c) Calculated  $hk1$  reflections. This pattern can never be observed as such in diffraction:  $hkl$  reflections can only be accessed in tilting experiments as illustrated in Figure 3.

developed again here. The structural consequences can be summarized in a simple statement. Either the helical hand (right (R) or left (L)) or the orientation (up (U) or down (D)) of two stems connected by a fold must be different, but they cannot differ both at the same time. In other words, LU and RD helices are not connected by a fold, but LU-RU or LU-LD may be connected by a fold. These constraints on helix chirality/clinicuity translate in observed unit-cell symmetries. LU and RD helices are linked by a center of symmetry. In the unit cells, centers of symmetry are, whenever possible, preferable since the structure tends to use the higher symmetry elements available. In chain axis projection, however, a unit cell that associates only one LU and one RD helix (with identical projections) would be perceived as a one-chain unit cell.

The observed doubling of the crystallographic  $a$ -axis as in  $\epsilon$ iPP is highly significant in the structure derivation. It determines the stem clinicuity/chirality organization and/or azimuthal setting and differentiates clearly the  $\epsilon$ iPP from the  $\alpha_2$ iPP structure.

**Structure Derivation:  $hk0$  Diffraction Pattern.** The unit cell, projected along the chain axis, has dimensions  $a = 12.50 \text{ \AA}$  and  $b = 24.6 \text{ \AA}$ . Compared to  $\alpha$ iPP ( $a = 6.55 \text{ \AA}$  and  $b = 20.78 \text{ \AA}$ ), the  $a$ -axis is nearly, but not quite, doubled, and the  $b$ -axis is nearly  $4 \text{ \AA}$  longer. These cell dimensions indicate that there are eight chains in the unit cell rather than only four for  $\alpha$ iPP. The cross section of the cell is  $308 \text{ \AA}^2$ , which translates in a stem cross-section area of  $38.4 \text{ \AA}^2$  ( $33.8 \text{ \AA}^2$  for  $\alpha$ iPP and  $35.2 \text{ \AA}^2$  for  $\beta$ iPP). The eight stems are organized in four layers distributed along the  $b$ -axis, with each layer along the  $a$ -axis being made of two stems with different projections.

In the initial stage of the structure derivation, it is convenient to consider only “simple” 3-fold iPP helices as they help grasp better the logics of the crystal structure. The stereodefects do not have a major impact on the diffraction pattern, although they are at the root of the different packing mode observed in this crystal structure.

The helical conformation needs first be established. The  $\approx 6.5 \text{ \AA}$   $c$ -axis parameter determined from relatively limited  $hkl$  information leaves many possibilities. The first ones to be considered are, given the large cross section, helices with more repeat units per turn than the standard 3-fold helices: 4-fold helices do have a  $6.5 \text{ \AA}$  periodicity. When considering a possible doubling of the  $c$ -axis repeat distance, a structure with  $7_2$  helices, as observed e.g. in poly(4-methylpentene-1) ( $c = 13.5 \text{ \AA}$ ) might be considered.<sup>14</sup> Oddly, it is the  $hk0$  reflections (i.e., looking *down* the helix axis) that indicate that these conformations can be ruled out. The  $c$ -axis projections of  $4_1$  and  $7_2$  helical are “too symmetric”. Whatever combinations of chirality/clinicuity and/or azimuthal settings are considered, these helices cannot explain the presence of the 060 reflection (Figure S3a,b). This leaves the “standard” 3-fold helical conformation of iPP as the only possibility and emphasizes the analogy with  $\alpha$ iPP, namely the sequence of layers along the  $b$ -axis. In  $\alpha$ iPP, due to their alternating antipolar azimuth settings, the helices in successive layers along  $b$  have their “tip” (lone methyl group) or their “base” (two methyl groups) oriented toward the  $+b$ -axis. These different helix orientations and the organization in four layers explain both the absence of the 020 and the presence of the 060 reflection (Figure 2b,c). The new structure must include a similar feature but must account also, in addition, for the doubling of the  $a$ -axis.

The major goal of the model building process is therefore to generate a reasonable organization of eight helices in a unit-cell with four layers along the  $b$ -axis, each layer being made of two stems along the  $a$ -axis. The helices differ, in chain axis projection, because of differences in helix chirality (right- or left-handed), helix orientation (up or down), and/or azimuthal setting (orientation relative to the  $a$ - and  $b$ -axes). Tentative models based on 3-fold helices have been constructed and tested for their agreement between calculated and observed  $hk0$  diffraction pattern and reasonable van der Waals contacts. There are many candidates that could fit in this pattern, mostly because  $hk0$  diffraction patterns cannot differentiate antichiral

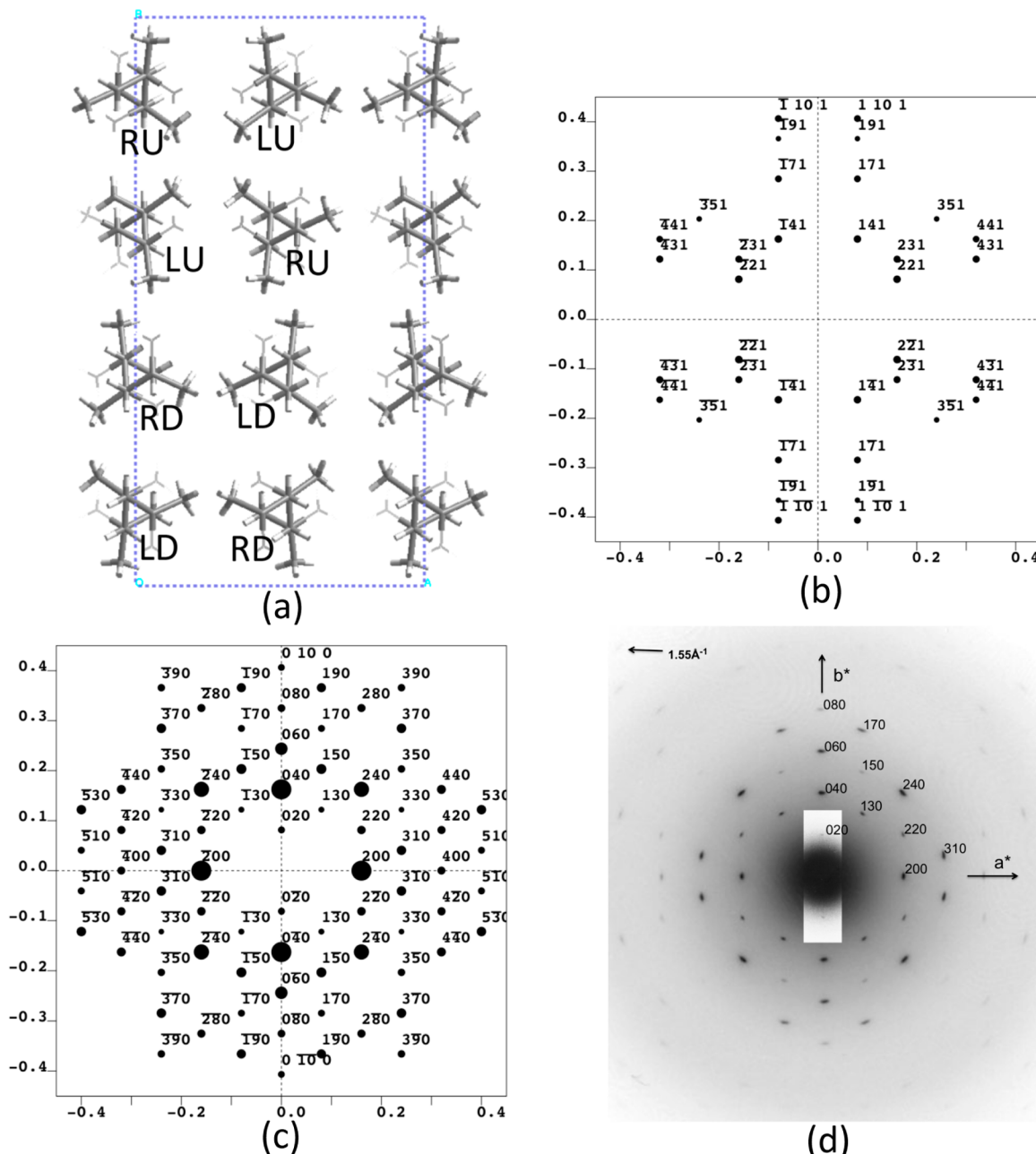


**Figure 5.** (a) Crystal structure of the stereodefective iPP  $\varepsilon$  phase. The cell dimensions and cell symmetry are as for Figure 4. The stereodefects are indicated with a lighter shading than the “standard” methyl side chains. (b) Calculated  $hk1$  reflections (not observable as such, cf. legend to Figure 4). (c) Calculated  $hk0$  diffraction pattern assuming a 10% concentration of stereodefects in the crystal structure. (d) Comparison with the experimental  $hk0$  electron diffraction pattern of an  $\varepsilon$ iPP single crystal.

anticline (e.g., RU and LD) helices. The monoclinic space group  $P2_1/c$  would be a suitable candidate. Among orthorhombic unit-cell symmetries, several space groups generate eight chains in the unit cell and obey the observed extinction rule for  $hk0$  reflections ( $h + k$  odd are extinct). (cf. also Figure S4).

The most plausible model of the  $\varepsilon$ iPP crystal structure (taking also into account the later  $hkl$  information) is shown in Figure 4. The calculated  $hk0$  electron diffraction pattern is displayed in part b and can be compared with the experimental one in Figure 2. The calculated pattern captures the essential features of the experimental diffraction pattern:  $h + k$  even, weakness/absence of 020, presence of 060, strength of the 040/200 and {240} reflections as well as presence of some critical

1 $k$ 0 and 3 $k$ 0 reflections that indicate doubling of the  $a$ -axis (130, 150, 170, 310). Some minor discrepancies between observed and calculated relative intensities indicate that there is still some room for improvement. However, considering the in-built uncertainties on intensities linked with electron diffraction and the limitations associated with the recording process, these discrepancies are likely to affect only secondary features of the model.

**Structure Derivation:  $hkl$  Reflections.** Given the impossibility to discriminate RU and LD helices in chain axis projection, a large number of combinations of eight chains with different helical hands/relative chain orientations and heights are compatible with the  $hk0$  single crystal diffraction data. They correspond to one monoclinic and several different

orthorhombic space groups. The monoclinic space group of interest in the present case is  $C2c$  (Figure S4, top). It is a familiar one. It describes the low-temperature  $\alpha_1$ iPP form, but in that case for a special position (the eight chains are located at four chain sites only, with both up and down stem orientations at each chain site). It is the only space group that would maintain a very close analogy between the  $\epsilon$ iPP and  $\alpha$ iPP crystal structures, namely the organization in four successive antichiral layers along the  $b$ -axis. The many orthorhombic space groups generate different combinations of helical hands and up/down orientations. In some space groups, the structure is best described as the succession of two clusters of four chains along the  $b$ -axis. Each cluster may be made of isochiral helices, with successive antichiral clusters along the  $b$ -axis (Figure S4, bottom). In other combinations, the cluster is made of two pairs of antichiral helices, each pair being located at opposite corners of the cluster. These different structural possibilities must be further compounded with up to three different relative heights of the helices or clusters.

A reliable discrimination between these various possibilities on the basis of three observed  $hkl$  reflections only is challenging. Fortunately, several potential candidates fail the test of the absence of extinction conditions on  $hkl$  reflections. It eliminates the monoclinic unit cell  $C2c$  space group and several orthorhombic ones (Figure S4). An extensive search closes down on the *orthorhombic space group  $Pccn$  as the most likely possibility*. It is the only space group that accounts for the presence and strength of the three observed  $hkl$  reflections, i.e., 141 and the 221–231 pair. These three reflections are among the most intense calculated on the first layer line using the “simple” 3-fold iPP helix (Figure 4c) as well as the later model that incorporates the stereodefects (Figure 5c)—they are even among the most intense diffraction spots of the powder pattern (cf. Supporting Information, Table). For most other space groups, the calculated diffraction pattern indicates that reflections of significant or sufficient intensity should appear in the tilted diffraction patterns since they are located near these three reflections (e.g., 041, Figure S4, bottom)). It should also be noted that for the  $Pccn$  space group that has been selected, there is an extinction rule for  $hk2$  reflections. No such reflections have been recorded in the tilting experiments, which would support the present assignment. However, this cannot be considered as an absolute selection criterion since the intensities expected for  $hk2$  reflections would be very weak in any case, and due to the limitation on the tilt angles of the tilting stage, only far out  $hk2$  reflections would be reached. Overall the  $Pccn$  space group is preferred, admittedly on limited, but in our view on sufficient experimental grounds. The calculated  $hkl$  reflections are displayed in Figure 4c and the calculated diffraction patterns for  $\approx 40^\circ$  tilts around both  $a$ - and  $b$ -axes of the single crystals are compared with the experimental ones in Figure 3a,b.

The structure of the different layers is thus as follows. In any one layer in the  $ac$  plane, neighbor helices are *antichiral* (right- and left-handed) but *isocline*—which accounts for their different projections (irrespective of their azimuthal setting). The next layer along the  $b$ -axis is made of the two same antichiral helices and the same clinicity, but shifted by one interstem distance along the  $a$ -axis and with an antipolar azimuthal setting to their counterparts. These four helices thus make up a quadruplet cluster of *isocline* helices: two right-handed and two left-handed ones located at opposite corners of the quadruplet. As a result, each helix has antichiral neighbors along both  $a$ - and  $b$ -axes.

Such a packing mode is a well-known and frequent feature in the structure of polyolefins (e.g., the Form I and III of isotactic poly(4-methyl-pentene-1)). In the present structure, however, this quadruplet is repeated along the  $b$ -axis, but this next quadruplet is oriented “upside down”, that is, anticline to the first one. This *succession of anticline double layers* is precisely the characteristic trademark of the  $\alpha_2$ iPP crystal structure. The  $\epsilon$ iPP structure is therefore an unusual combination of on one hand *clusters of four antichiral isocline helices* that mimics the tetragonal packing of many isotactic polyolefins and on the other hand of the more specific succession of *anticline double layers* observed in the  $\alpha_2$ iPP crystal structure. As such, it is a packing mode never observed so far in any crystal structure of isotactic polyolefins.

**Structure Derivation: Impact of Stereodefects and Steric Conflicts.** The simple isotactic iPP model considered so far helps grasp the complex organization of the 3-fold helices in the  $\epsilon$ iPP crystal structure. The peculiarities of this structure are however linked with the presence of stereodefects. We will consider only simple *mmrrmm* stereodefects that result in an interchange of the positions of the methyl group and the hydrogen atom linked to the same main chain carbon. As a result, the stereodefective methyl groups are located close to the helix axis rather than projecting outward (Figure 5a). However, for probably rather low densities of stereodefects, the impact on the diffraction pattern is limited, as illustrated by Figure 5b,c. These  $hk0$  and  $hk1$  patterns, calculated for an iPP in which 10% of the repeat units are stereodefective, are essentially similar to the ones shown for “pure” iPP in Figure 4b,c. This similarity results from the fact that, when taking also into account the main chain atoms, the 10% figure means that only  $\approx 3\%$  of the carbon atoms in the structure have a different location. The model illustrated in Figure 5 (atomic coordinates in Table S8) features a rotation of the chains on their axes compared to the “pure” defect-free iPP in order to reach a better (again, qualitative) agreement with the diffraction pattern.

The absence of interstem steric conflicts is an additional meaningful criterion in assessing the validity of any structural model. This criterion is easy to evaluate when the symmetry of the helix matches that of the unit cell. It becomes more cumbersome when these symmetries are different, in particular for irrational helices that must pack in “standard” hexagonal or tetragonal unit cells. Usually, short contacts are unavoidable when considering fixed, undeformed helical symmetries. In the present case, the impact of stereodefects may result in local steric adjustments, which creates an extra difficulty. It is thus, again, useful to consider first the stereodefect-free situation.

For the *defect-free* 3-fold helices illustrated in Figure 4, and as expected from the large cross section available to each stem, the shorter interstem contacts (between  $\text{CH}_2$  and  $\text{CH}_3$ ) are at a comfortable 3.7–3.9 Å, slightly more than the sum of the van der Waals radii. The shorter methyl–methyl contacts are about 4 Å, an accepted low limit. Most of them are usually at 4.5 Å or more. This extra interstem space is clearly devoted to accommodate the stereodefects.

Incorporation of stereodefects does result in some local steric conflicts. The shorter  $\text{CH}_3–\text{C}'\text{H}_3$  distances ( $\text{C}'\text{H}_3$  stands for the stereodefective methyl) are  $\approx 3.10$  Å, a value definitely below the accepted lower limit of 4 or  $\approx 3.8$  Å (Figure S7). A short 3.10 Å distance would be unacceptable if all the  $\text{C}'\text{H}_3$  sites were occupied. These short contacts illustrate the fact that even though the stem cross section is expanded, the packing of

these helices experiences constraints similar to those of irrational helices. Whatever the structure considered, accommodation of stereodefects requires local conformational adjustments.

## ■ DISCUSSION

The structural model derived for the  $\epsilon$  phase of stereodefective iPP, even though it has not reached full maturity, captures its essential and most original features. These features provide interesting insights into the stereodefects and their structural consequences in terms of chain conformation or chain packing, which result in a crystalline density 2% lower than the amorphous phase. They also shed new light on the specificity of the iPP  $\alpha$  and  $\gamma$  crystal structures.

**Nature of the Stereodefects.** The topic of the nature and impact of stereodefects and comonomers on iPP molecular conformation and crystal structure has been investigated extensively in the past decades. The reader is referred in particular to the comprehensive work performed in Italy, neatly reviewed in a recent paper by De Rosa et al.<sup>18</sup> on the role of stereodefects and comonomers (with ethylene or butene) on the crystal polymorphism of iPP—limited, of course, to the generation of  $\alpha$  and  $\gamma$  iPP phases. Some simple guidelines need however to be mentioned in the present context.

The stereodefects considered in the present structure derivation are only “wrong” placements of the methyl side chains. Such defects result from the presence of  $rr$  triads in an  $mmmm$  polymer chain:  $mmrrmm\dots$ . They are *local* defects that may be incorporated in a crystal structure and, more importantly, do not change the sense of spiralization of the helix. Indeed, the *rather stringent interplay/alternation of helical hands* along both  $a$  and  $b$  crystal axes imposed by the  $Pccn$  space group *does not allow for uncontrolled helical hand reversal*.

The  $rr$  triads have been recognized to induce the  $\gamma$ iPP phase in many earlier investigations of stereodefective iPPs. De Rosa et al. have considered two different conformations that may be generated by such stereodefects.<sup>19</sup> The first model is similar to the one considered here: the defect maintains the helix chirality and helix axis. The second model implies helical hand reversal and helix bending leading to a reorientation of the helix axis by  $\approx 80^\circ$ . It was suggested that it might be incorporated in the  $\gamma$  crystal lattice and  $\alpha/\gamma$  disordered modifications of iPP since helix orientations  $\approx 80^\circ$  apart exist in  $\alpha/\alpha$  lamellar branching and in the  $\gamma$ iPP crystal structure. The strict parallelism of helices and absence of uncontrolled helical hand reversal in  $\epsilon$ iPP appears to exclude this second structural model in the present case. Along the same line, it excludes the incorporation in the crystal lattice of defects of  $mnmrm$  type that would result in a helical hand reversal: such defects are most probably rejected in the crystal/amorphous interlayer.

Whereas the nature of the stereodefects leaves little doubt, their concentration remains a totally open issue. The experimental evidence suggests that under the crystallization conditions used—very slow cooling of thin films—the iPP used here crystallizes a little in the  $\alpha$ , much more in the  $\gamma$ , and very marginally in the  $\epsilon$  phase.

A tentative guideline for possible stereodefects concentrations compatible with  $\epsilon$ iPP formation would be to assume that iPPs that crystallize in  $\alpha/\gamma$  mixed crystals or in “pure”  $\gamma$  phase can also form the new phase. This criterion is however a very blunt one, as the  $\gamma$  phase is obtained for a wide range of stereodefective iPPs. As indicated by the early results of Turner-Jones et al.<sup>20</sup> and the studies of Rieger et al.<sup>7</sup> confirmed by all

later investigations,<sup>21</sup>  $\gamma$ iPP is present or is the major phase for  $rr$  percentages ranging from 80 or 90% down to 50 or even 35% (cf. Figure S1). The modeling of the diffraction pattern of Figure 5 *assumes* a 10% stereodefects concentration. This percentage would correspond to a  $mmmm$  content of 50%, or one stereodefect for every ten monomers units. In crystallographic terms, this would represent one defect for every three turns or every  $\approx 20$  Å along the helix axis. In addition, these defects are distributed over three positions in the helix, which would translate in less than two stereodefects for each of the three sides of the stem in a chain folded crystal 10 nm thick. Let us remind however that the 10% stereodefects figure used here is only indicative: assumed higher defects concentrations would still be compatible with the diffraction evidence gathered in this work.

Additional segregation mechanisms that would reduce the concentration of defects within the crystal lattice as compared to the original material are certainly operative. The first one is the well-documented rejection of stereodefects outside the crystalline lamella and into the fold surface. This “morphological partitioning” in the words of VanderHardt et al.<sup>22</sup> (here “morphology” means crystalline core versus amorphous interlayers) has been quantified for metallocene iPPs crystallizing in the  $\alpha$  and  $\gamma$  modifications. “Definite [NMR] defect-resonance patterns associated with both the simple  $mrrm$  stereodefect and the regio 2,1-erythro defect have been identified.” On the basis of various arguments and assumptions made by these authors, “the following values were obtained: PCR(stereo:  $mrrm$ ) =  $0.48 \pm 0.06$  and PCR(regio: 2,1-erythro) =  $0.28 \pm 0.08$ .” In other words, the concentration of  $mrrm$  defects within the crystal lattice is nearly half of the value expected were the defects uniformly distributed over the amorphous and crystalline parts. The results indicate “there is only a weak dependence, if any, on kinetics or crystal habit.” The authors also suggest “those defects seen in the crystal spectrum are highly concentrated at the crystal/non-crystalline interface”.<sup>22</sup> A similar partitioning is more than likely for the present  $\epsilon$ iPP phase (and would reduce the  $mmmm$  content of the initial material to 35% in order to reach a 10% defects concentration in the crystal lattice). It may be less marked however: in an expanded crystal lattice, the driving force for such a morphological partitioning is lower.

A likely second mechanism is the molecular segregation mentioned earlier: the most stereodefective parts of the material crystallize later than the less defective ones. This possibility is suggested by the delayed  $\alpha-\epsilon$  growth transition observed in some of the crystals and would correspond to a “crystal phase” partitioning but appears to be contradicted by the earlier NMR results that suggest “only a weak dependence on crystal habit”.<sup>22</sup>

At any rate, no definitive conclusion regarding the concentration of stereodefects needed to induce and stabilize this  $\epsilon$  crystal modification of iPP can be drawn at the present time and probably will not be drawn before a bulk material with a significant amount of  $\epsilon$ iPP phase is obtained and subjected to extensive crystallographic and NMR investigations. These studies must focus in particular on the “morphological partitioning” mentioned earlier, which is definitely a significant issue when investigating highly stereodefective materials.

**Impact of Stereodefects: Chain Conformation and Near-Tetragonal Packing of 3-Fold Helices.** The chain conformation of the  $\epsilon$ iPP phase remains a 3-fold helix in spite of the presence of stereodefects. A comparison with the

structure of polyisobutylene (PisoBu) is appropriate, since in this polymer the steric conflicts associated with the presence and similar location of the extra methyl group are a systematic feature.

Accommodation of the extra methyl group in the PisoBu helix results in an increase of the C–C(H<sub>2</sub>)–C valence angle. Benedetti et al. determined a value of 122° from the structure of the low molecular weight model compound 2,2,4,4-tetramethyladipic acid.<sup>23</sup> Tanaka et al. report values closer to 130° in their structure analysis of PisoBu.<sup>24</sup> Compared to iPP, the helix “unwinds”: it becomes a 8<sub>3</sub> helix (9<sub>3</sub> or 3<sub>1</sub> helix for iPP). The rotation per residue increases from 120° to 135°. This unwinding results from the location of the extra methyl group close to the helix axis. Steric repulsions push the backbone C(H) carbon away from the helix axis, thus leading to a more “open” helical path. The helix is also expanded in the chain axis direction: three repeat units span 7 Å along the c-axis in PisoBu as opposed to 6.5 Å for iPP.<sup>24–26</sup>

In the stereodefective iPP, both the 3-fold helix symmetry and the 6.5 Å periodicity are maintained. Whereas local deformations, in particular of the C–C(H<sub>2</sub>)–C valence angle, are likely (this valence angle appears to bear most of the conformational load), the stereodefects are sufficiently “diluted” and do not modify the helix conformation. They have however a major impact on their packing.

Packing of 3-fold helices in a nearly tetragonal arrangement is counterintuitive, to say the least. In its simplest form, considering the chain axis projections, why should triangles pack on a square lattice? The answer to this puzzling feature must lie in the impact of the different location of stereodefects. When repeated for a sufficient number of stereodefective methyls along the helical stem, the overall helix shape changes considerably. Although it retains its 3-fold symmetry, its c-axis projection is more “rounded” and approaches that of “less crystallographic” or irrational helices that pack frequently (but not exclusively) in tetragonal unit cells (Figure 6).

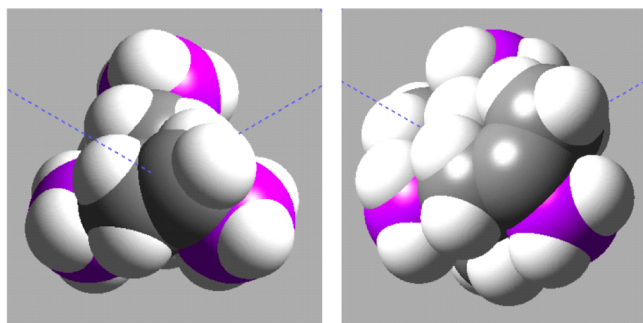


**Figure 6.** The c-axis projection of an iPP 3-fold helix (left) and the same helix in which all possible stereodefect sites are occupied. The methyl carbons are purple for “standard” methyls and gray for the stereodefects. Only a fraction of the latter sites are occupied in the present material. The full van der Waals radii are used here. They convey better the encumbrance introduced by the stereodefects and the resulting overall rounder shape of the helix.

Stereodefects can be accommodated within the  $\alpha$ iPP and even better so in  $\gamma$ iPP phases. Generation of this different  $\epsilon$ iPP structure indicates that a concentration threshold has been exceeded. Conversely, however, once it has been generated, it appears to be a preferred packing mode for stereodefective iPP, as suggested by Figure 1b.

### Doubling of the *a*-Axis, Cell Symmetry, and Crystal Morphology.

The  $\epsilon$ iPP phase displays many features of the  $\alpha$ iPP one, with the notable exception of the doubling of the *a*-axis parameter. The *Pccn* space group indicates that this doubling is not merely the result of a different azimuthal setting of an  $\alpha$ iPP-like structure made of isochiral *ac* layers, but reflects a genuine alternation of helix chirality along the *a*-axis. This doubling must be considered within the more general context of possible conformations, cell symmetry, constraints on chain folding, and related crystal morphology of isotactic polyolefins.

The crystal structures of many isotactic polyolefins have lower symmetry than would be possible if the centers of symmetry associated with LU-RD organization were allowed. Numerous examples are found in e.g. the tetragonal unit cells of Form II of poly(1-butene) or Form I of poly(4-methyl pentene-1). In all these cases, alternation of different chain axis projections introduces a doubling of the *a* and *b* parameters, which translates in an alternation of antichiral isocline (RU-LU) or of isochiral anticline (LU-LD) stems. The same observation applies even for unit cells with lower symmetry. For the monoclinic Form II of iP4MP1 made of helices with 4-fold symmetry, a doubling of the *a* parameter, only detected via weak reflections in the electron diffraction pattern of single crystals, indicates also an alternation of isochiral anticline helices in the major growth faces.<sup>27</sup> Also, isochiral crystal structures of isotactic polyolefins, such as the orthorhombic Form III of iPBu, have in-built screw axes (in this specific case the *P2<sub>1</sub>2<sub>1</sub>2<sub>1</sub>* space group) which impose that adjacent isochiral stems are anticline in the {110} growth faces.

The crystal structure of  $\alpha_2$ iPP stands in sharp contrast with the above, rather general pattern and raises problems that remain open. The succession of layers along the *b*-axis in  $\alpha_2$ iPP is RU, LU, RD, LD. As analyzed by Petraccone et al.,<sup>16</sup> chain folding within any one *ac* layer does not obey the constraints rule. It is not possible also between LU and RD layers that are linked by a center of symmetry. It is only possible *between* the layers that build the RU-LU and RD-LD bilayers. In other words, folds would “knit” together the two layers parallel to the *a*-axis and made of antichiral but isocline stems. This folding pattern would privilege the {110} planes as growth planes, as is indeed suggested by polymer decoration on solution-grown single crystals. At any rate, the shape of iPP crystals depends significantly on the crystallization conditions, and most notably on *T<sub>c</sub>*.

The novel element introduced by the present investigation is that a high temperature crystal habit very similar to  $\alpha_2$ iPP is obtained when the stems within any single *ac* or *bc* layer are antichiral but isocline, i.e., allow folding within the layer. In this sense, the “quadruplet” structure does not differentiate the *a*- and *b*-axes, which should result in comparable growth rates in the two orthogonal directions, as is the case for tetragonal cell symmetries. This is not the case: the  $\epsilon$ iPP crystals are elongated in the *a*-axis direction, which implies a specific hindrance to the growth in the *b*-axis direction. This hindrance appears to be the center of symmetry that exists in both  $\alpha$ iPP and  $\epsilon$ iPP unit cells and would support Petraccone et al.’s analysis on the restrictions generated by the folds in isotactic polyolefins. More generally, it would appear that centers of symmetry in the unit cells of isotactic polyolefins are hardly compatible with chain folding. If the centers of symmetry exist, the crystal morphology does not reflect the unit-cell symmetry (as it should do), but reflects the conformational hindrances imposed by the folding pattern.

**Finalizing the  $\epsilon$ iPP Crystal Structure.** As repeatedly indicated, the structure analysis of  $\epsilon$ iPP developed in this work probably leads to a first-order model that may be improved. It should be emphasized again that the present structure derivation rests on data obtained from a limited number of single crystals (which taken together amount probably to less than 1 ng of material). Also, the structural model rests for the most part on a limited number of indicators—in essence four reflections: strength of the equatorial 060 (and concomitant weakness of 020) and the three major  $hkl$  reflections: 141, 221, and 231. Information provided by additional  $hkl$  reflections would be very useful in finalizing the details of the structure.

Possible improvements, already mentioned, may deal with the helix geometry and the local perturbations introduced in the vicinity of the stereodefects. This will become possible only if and when significant amounts of this material, preferably “unspoiled” by  $\alpha$ iPP and  $\gamma$ iPP become available—*a priori* a very difficult experimental challenge.

Improvements of the suggested packing should also be considered. Although the comparison of calculated and experimental diffraction intensities remains qualitative, the relative calculated intensities of some sets of  $hk0$  reflections need to be improved. This holds for example for 130, 150, and 170 reflections: 130 remains rather weak whatever positional adjustments are attempted within the orthorhombic symmetry. Relieving the short contacts would be helped by positional adjustments of the stems in the cell. The orthorhombic symmetry with well-defined positions of the chains in the unit cell may need to be relaxed.

A monoclinic cell symmetry would provide more freedom in these adjustments. The  $C2c$  space group of  $\alpha_1$ iPP is—was—a tempting candidate. It generates eight stems and would perfectly explain the morphological similarity of  $\alpha$ iPP and  $\epsilon$ iPP but is ruled out by the extinction conditions on the first layer line (Figure S4, top).

A crystal structure with  $Pccn$  space group implies that each of the eight stems has a specific chirality, up or down orientation relative to its neighbors (clinicity) and defined azimuthal setting relative to the  $a$ - and  $b$ -axes. These characteristics remind the  $\alpha_2$ iPP crystal structure. In  $\alpha$ iPP, two variants exist that differ only by the relative orientation of stems: the up–down condition is relaxed in  $\alpha_1$ iPP, which is described as a statistical structure with eight stems and half-occupancy at each site. A similar up–down disorder is conceivable in  $\epsilon$ iPP since, also, it would maintain the chirality and azimuthal setting of the stems. In other words, whereas the present structure would correspond to  $\epsilon_2$ iPP, does a “sister”  $\epsilon_1$ iPP crystal structure exist? The unit cell of such an  $\epsilon'$ iPP crystal phase would contain 16 stems shared between eight sites with half-occupancy at each site. A number of orthorhombic space groups generate 16 stems, but they do not support the possibility of up–down disorder in  $\epsilon$ iPP. In all these space groups, there are conditions on  $hk0$  reflections that are not met and/or conditions on  $hkl$  reflections that are incompatible with the presence of both 221 and 231 reflections (see also Figure S6 that illustrates another packing mode that has been discarded).

**$\alpha$ iPP,  $\gamma$ iPP, and  $\epsilon$ iPP Structures for Stereodefective IPP.** The  $\epsilon$ iPP structure is in essence a structural alternative for, probably, highly stereodefective iPP and may well be the ultimate structure before the material turns amorphous. High concentration of defects implies lower melting and crystallization temperatures, which may explain also, at least partly, the delayed appearance of  $\epsilon$ iPP in crystallization experiments

that involve slow cooling. However, the uncovering of this new crystal structure does not break the accepted dogma: the favored iPP crystal phase for stereodefective iPP remains  $\gamma$ iPP and to a more limited extent  $\alpha$ iPP.

Observation of a crystal structure with a higher stem cross section to accommodate stereodefects is not a surprise. However, it raises issues regarding the “accepted dogma” about  $\alpha$ iPP and  $\gamma$ iPP being hosts of stereodefects. On what structural grounds can  $\alpha$ iPP house stereodefects? Also, why is  $\gamma$ iPP a better host for stereodefects than  $\alpha$ iPP in spite of the fact that it is the densest of all known iPP crystal structures? The answer may involve many factors, but in a first approach the ease with which the structure houses the stereodefects needs be estimated. It is known that stereodefects tend to expand the lattice of  $\gamma$ iPP. The steric conflicts introduced by stereodefects can be mapped using a procedure already applied for  $\epsilon$ iPP. The result is shown in Figure S7 for  $\alpha$ iPP and  $\gamma$ iPP.  $\text{CH}_3\text{--C}'\text{H}_3$  distances remain on the short side, as would be expected, but a major structural feature emerges: when in  $\alpha$ iPP the 3-fold helices interact via their “flat” faces, that is, across the glide planes parallel to the  $ac$  plane, introduction of stereodefects generates prohibitively short steric contacts (here, typically,  $\approx 3$  Å). On the other side of the 040 layers, when the tips of 3-fold helices interdigitate, the accommodation of stereodefects is by comparison much easier: the different potential locations for stereodefects are not equal. This observation suggests a possible selection mechanism based on adequate azimuthal adjustment of the stems in the  $\alpha$ iPP and, similarly,  $\gamma$ iPP phases. For low concentrations of stereodefects, the azimuthal setting adopted by the stems could be such as to position the stereodefects at the more favorable locations. (This effect should not however affect significantly the separation of the layers and bilayers, as it would generate a 020 reflection that is not observed in the powder patterns of these materials.<sup>7</sup>) By extension also, when the concentration of the stereodefects is further increased, the “difficult” sites (or a significant proportion of them) must be occupied. The short  $\approx 5.2$  Å interhelix distance in  $\alpha$ iPP and  $\gamma$ iPP becomes untenable. The structure switches to the  $\epsilon$ iPP structure with its more “symmetrical” interstem interactions and larger interstem distance ( $\approx 6.2$  Å) for nearly similar relative azimuthal orientation of the two antichiral stems, this time along the  $a$ -axis.

**Metastability and Potential of the  $\epsilon$ iPP Structure.** The characteristics of  $\epsilon$ iPP indicate a metastable phase. The major and most distinctive feature of  $\epsilon$ iPP is its *low density* (0.838 g/cm<sup>3</sup>),  $\approx 10.7\%$  and  $\approx 11.9\%$  lower than for  $\alpha$ iPP or  $\gamma$ iPP phases (0.938 and 0.951 g/cm<sup>3</sup>, respectively) and also 8.7% lower than  $\beta$ iPP (0.918 g/cm<sup>3</sup>) and even, as already indicated, 2% lower than that of the amorphous phase (0.855 g/cm<sup>3</sup>). Of course, some crystal structures of polyolefins are known to have a density lower than that of their amorphous phase (e.g., poly(4-methyl-pentene-1), the  $\alpha$  phase of syndiotactic polystyrene). In the present phase, this low-density results from two features: (a) half of the potential sites of side chains are not occupied, and (b) the cell geometry is not adapted to 3-fold helices. The relative impact of these features and other related aspects associated with metastability may be evaluated by comparison with relevant crystal structures of iPP and iPBu1.

The major reason for the *low density* is linked with the existence of unoccupied sites, as indicated by a comparison with  $\delta$ iPP. This form is generated when 10–20% of propylene units are replaced by hexene ones. It is structurally similar to the

trigonal Form I of iPBu1, which enables housing of the extra side-chain material introduced by the comonomer. For 10% hexane counits, the unit cell is slightly smaller than that of iPBu1 (the  $a$  parameter is 17.17 Å vs 17.7 Å), but the copolymer crystallizes in the iPBu1 Form I crystal structure type even though, overall, 35% of the side chain material present in iPBu1 is missing. The density of this copolymer is thus only 0.832 g/cm<sup>3</sup>, about 14% lower than the “normal” iPBu1 Form I one (0.95 g/cm<sup>3</sup>), or in other words, a sample with 82.5% of the material is housed in a cell 94% the volume of that of iPBu1. For both  $\delta$ iPP and  $\epsilon$ iPP “unoccupied” sites thus result in densities significantly lower than those of the stable phases.

The impact of the adequate or inadequate matching of cell geometry and helix symmetry also plays a—more limited—role. For  $\delta$ iPP, the near-tetragonal cell symmetry is a “by default” choice and is not adequate to house 3-fold helices. A measure of this impact is provided by a comparison with iPBu1 Form I (trigonal cell,  $a = b = 17.7$  Å,  $c = 6.5$  Å, six 3-fold helices) and of Form II (tetragonal unit cell,  $a = b = 14.85$  Å,  $c = 20.6$  Å, four irrational 11<sub>3</sub> helices).<sup>28</sup> Their densities are 0.950 and 0.9024 g/cm<sup>3</sup>, respectively. The inadequate helix conformation in Form II therefore results in a ≈5% lowering of the crystal density compared to the stable phase.<sup>29</sup> It is clear that in the  $\epsilon$ iPP crystal structure the combination of the unoccupied sites and the inappropriate helix symmetry add up and result in the observed low crystal density.

In addition to lower densities, metastable crystal phases have usually also *faster growth rates* than the corresponding stable phases. Here again, a comparison with Form I and Form II of iPBu1 is of interest. The growth rate of the metastable Form II is known to be significantly faster than for Form I. The limited evidence available suggests that this holds true also for  $\epsilon$ iPP, although quantitative data are missing.

The *nucleation processes* of  $\epsilon$ iPP and iPBu Form II are however significantly different. iPBu Form II is formed spontaneously on cooling the melt and grows faster than the other phases. Materials in nearly pure iPBu Form II can thus be obtained and tested for their mechanical properties.  $\epsilon$ iPP has been observed so far to nucleate mostly or only via a crystal-crystal transition from a pre-existing  $\alpha$ iPP phase. Reaching high concentrations of this phase would require as a prerequisite the development of  $\epsilon$ iPP-specific nucleating agents used in addition with polymers with a chemical constitution (to be determined) more prone to yield this phase.

Going on with this comparison with iPBu, it should be noted that  $\epsilon$ iPP may well avoid the well-known long-term *structural instability* of iPBu1 Form II. This phase is known to transform spontaneously over time ( $\approx 1$  week) to the more stable and denser Form I, which limits its industrial interest, especially in injection molding.<sup>30</sup> The transformation has been analyzed at the molecular level.<sup>31</sup> It implies a change from the 11<sub>3</sub> helical conformation to the more stable 3<sub>1</sub>, a transformation that *maintains* the helical hand of each stem. The transformation is possible because Form I and Form II are *both* made of alternating antichiral layers made of isochiral helices: the crystal-crystal transformation is relatively “easy” since it does not imply helical hand reversal and thus major reshuffling of the crystal structure.

A similar *spontaneous* solid-state transformation involving  $\epsilon$ iPP appears less likely. The crystallographic characteristics of this phase differ too much from the potential target structures:  $\alpha$ iPP or  $\gamma$ iPP. In  $\gamma$ iPP, the most likely final structure (since it is

the major phase of stereodefective iPP), the chains axes are not parallel, which renders a solid-solid transformation virtually impossible. Only a melting-recrystallization process would do. In a similar manner a  $\epsilon$ iPP- $\alpha$ iPP transformation appears unlikely even though the chains axes would remain parallel. First,  $\alpha$ iPP is not the preferred crystal structure of stereodefective iPP and therefore not the natural target in a transformation—it may not be a target at all. Second, the structures are different in the helical hands involved: for comparable interstem distances in the ac layer, neighbor stems are isochiral in  $\alpha$ iPP and antichiral in  $\epsilon$ iPP.

The structural hindrances to solid-solid phase transformations of  $\epsilon$ iPP would alleviate the long-term problems encountered by iPBu1 in injection-molding.  $\epsilon$ iPP would however retain its major advantage, namely a ≈11% lower crystalline density than  $\alpha$ iPP or  $\gamma$ iPP. For an overall 50% crystallinity, this difference would translate in a ≈5% lower overall density. (This view is probably overly optimistic. Injection molding generates mechanically induced nucleation that would be of  $\alpha$ iPP, with additional growth in the equally dense  $\gamma$ iPP.) Lower densities are usually associated with poorer mechanical properties, as illustrated by HDPE and LDPE. In LDPE, the poorer mechanical properties result from a higher fraction of *amorphous* material. In a similar way, the “structural-mechanical phase diagram of isotactic polypropylene” provided by De Rosa and Auriemma<sup>32</sup> indicates that the elastic properties of stereodefective iPP are linked with a significant proportion of amorphous material with “crystalline domains acting as knots of the elastomeric network”.  $\epsilon$ iPP, on the contrary, is a lower density *crystalline* material that can incorporate higher concentrations of stereodefects, thus resulting in a higher crystallinity for the same material. If and when such a “lightweight”  $\epsilon$ iPP can be produced (via proper adjustment and control of the stereochemistry, processing conditions and/or specific nucleating agents, etc.), the resulting material would probably have higher stiffness. At the same time, and in view of its low density,  $\epsilon$ iPP, much like  $\beta$ iPP, would probably display low resistance to *mechanically induced* (as opposed to spontaneous) transformations.

Finally, and to conclude with the parallel between iPP and iPBu1, let us point out a pleasant but also major difference between the two materials. In the present work, it has been shown that the presence of stereodefects in iPP induces a metastable, even if elusive  $\epsilon$ iPP phase with low density. By contrast, the impact of stereodefects on the iPBu1 polymorphism is exactly opposite. As shown by de Rosa et al.,<sup>33</sup> stereodefective iPBu crystallizes directly in the stable Form I rather than in the “conventional”, metastable Form II. It would appear that there is no single way for polyolefins to deal with stereodefects. On a structural basis, however, this difference makes sense. Inclusion of stereodefects induces an unwinding of the helix, as illustrated by the comparison of iPP and polyisobutylene. In iPBu1, the metastable Form II 11<sub>3</sub> helix has an azimuthal rotation per residue of ≈98° compared to 120° for the 3-fold helix of the stable Form I. The stereodefects in iPBu1 thus merely induce a more “open” helix that happens to be that of the stable crystal modification.

## CONCLUSION

The major features of an original crystal phase specific to stereodefective iPP have been established on the basis of single crystal electron diffraction data. Observation of an original crystal structure of isotactic polypropylene comes as a surprise

considering the many years devoted to structural investigations of iPP and, more recently, to stereodefective iPPs. This structure is in any case only a very minor component of the material used and thus would not have been detected by global investigation means. It is characterized by a number of original structural features that contribute to a better understanding of the rich polymorphism of isotactic polypropylene(s).

The chain conformation remains the archetypical 3-fold helix of all the known phases of iPP. However, stereodefects of the type *mmrrmm* generate a location of the methyl group similar to that observed in polyisobutylene. As a result, the *c*-axis projection of the 3-fold helix mimics to some extent that of irrational helices and the packing becomes tetragonal-like. The unit cell is highly original in polymer crystallography. In essence, it is very nearly a “double tetragonal” unit cell with a succession of two anticline clusters of four chains along the *b*-axis. The clusters’ structure is similar to that observed in tetragonal unit cells of polyolefins: the four helices are isoclinal but antichiral along both *a*- and *b*-axes; each helix is thus surrounded by four antichiral neighbors.

Stereodefective iPPs were so far known to crystallize mostly in the  $\gamma$  phase.  $\epsilon$ iPP illustrates yet a different, more drastic structural response that is required when the concentration of stereodefects becomes no longer compatible with their uncomfortable “squeezing” in the dense  $\alpha$  or  $\gamma$  phases (even if with expanded cell dimensions). Elucidation of this new phase is mostly of fundamental interest. Further work should be devoted to better determine the concentration window of stereodefects and crystallization conditions for which this phase is generated. More effective nucleation mechanisms than the mere crystal–crystal growth transition from  $\alpha$ iPP or, even better, efficient  $\epsilon$ iPP-selective nucleating agents should be designed. They may open the way to possible applications that take advantage of the  $\epsilon$ iPP’s  $\approx 11\%$  lower crystal density than  $\alpha$ iPP or  $\gamma$ iPP.

## ASSOCIATED CONTENT

### Supporting Information

Figure S1: electron micrograph of bent quadrates of stereodefective iPP; Figure S2: sketch of the structure of composite  $\alpha/\gamma$  single crystals grown in thin film; Figure S3: crystal structures (discarded) based on  $4_1$  and  $7_2$  helices and their calculated  $hk0$  diffraction patterns; Figure S4: crystal structures (discarded) based on  $3_1$  helices with the monoclinic space group  $C2c$  and orthorhombic space group  $Pbcn$ , their calculated  $hk0$  diffraction patterns and  $hk1$  reflections; Table S5a: Structure determination; observed and calculated spacings of major  $hk0$  and  $hkl$  reflections; Figure S5b: comparison of the calculated X-ray powder diffraction patterns of the  $\alpha$ ,  $\gamma$ , and  $\epsilon$  crystal phases of iPP; Table S5c: major reflections calculated for the powder patterns of the  $\epsilon$  and, for comparison purposes,  $\alpha$  and  $\gamma$  phases of isotactic polypropylene; Figure S6: scheme of the V-amylose complex with an original tessellation also considered in this structure derivation; Figure S7: diagrams of short contacts in the  $\alpha$ ,  $\gamma$ , and  $\epsilon$  crystal structures of stereodefective iPP; Table S8: atomic coordinates of the  $\epsilon$ iPP crystal structure. This material is available free of charge via the Internet at <http://pubs.acs.org>.

## AUTHOR INFORMATION

### Corresponding Author

\*E-mail bernard.lotz@ics-cnrs.unistra.fr.

## Notes

The authors declare no competing financial interest.

## ACKNOWLEDGMENTS

I thank Professor J. C. W. Chien, University of Amherst (retired), for providing the sample used in the present investigation and apologize to him for the long delay it took to finalize this work. I thank also Pr. B. Rieger, Technical University of Munich, for providing more recently other sets of stereodefective iPP samples that are still under investigation. Very constructive criticisms and comments of the editors and reviewers are also acknowledged.

## REFERENCES

- (a) Brückner, S.; Meille, S. V.; Petraccone, V.; Pirozzi, B. *Prog. Polym. Sci.* **1991**, *16*, 361–404. (b) Lotz, B.; Wittmann, J. C.; Lovinger, A. J. *Polymer* **1996**, *37*, 4979–4992.
- (2) Natta, G.; Corradini, P. *Nuovo Cimento, Suppl.* **1960**, *15*, 40–51.
- (3) (a) Khouri, F. J. *Res. Natl. Bur. Std., Sect. A* **1966**, *70A*, 29–61.
- (b) Padden, F. J.; Keith, H. D. *J. Appl. Phys.* **1966**, *37*, 4013–4020.
- (c) Binsbergen, F. L.; De Lange, B. G. M. *Polymer* **1968**, *9*, 23–40.
- (d) Lotz, B.; Wittmann, J. C. *J. Polym. Sci., Part B: Polym. Phys.* **1986**, *24*, 1541–1558.
- (4) (a) Brückner, S.; Meille, S. V. *Nature* **1989**, *340*, 455–457. (b) Meille, S. V.; Brückner, S.; Porzio, W. *Macromolecules* **1990**, *23*, 4114–4121. (c) Ferro, D. R.; Brückner, S.; Meille, S. V.; Ragazzi, M. *Macromolecules* **1992**, *25*, 5231–5235.
- (5) (a) Lotz, B.; Kopp, S.; Dorset, D. *C. R. Acad. Sci. Paris* **1994**, *319*, 187–192. (b) Meille, S. V.; Ferro, D. R.; Brückner, S.; Lovinger, A. J.; Padden, F. J. *Macromolecules* **1994**, *27*, 2615–2622. (c) Dorset, D. L.; McCourt, M. P.; Kopp, S.; Schumacher, M.; Okihara, T.; Lotz, B. *Polymer* **1998**, *39*, 6331–6337. (d) Stocker, W.; Schumacher, M.; Graff, S.; Thierry, A.; Wittmann, J. C.; Lotz, B. *Macromolecules* **1998**, *31*, 807–814. (e) Ferro, D.; Meille, S. V.; Brückner, S. *Macromolecules* **1998**, *31*, 6926–6934.
- (6) (a) Lotz, B.; Ruan, J., Jr.; Thierry, A.; Alfonso, G. C.; Hiltner, A.; Baer, E.; Piorkowska, E.; Galeski, A. *Macromolecules* **2006**, *39*, 5777–5781. (b) De Rosa, C.; Auriemma, F.; Corradini, P.; Tarallo, O.; Dello Iacono, S.; Ciaccia, E.; Resconi, L. *J. Am. Chem. Soc.* **2006**, *128*, 80–81. (c) De Rosa, C.; Auriemma, F.; Talarico, G.; Ruiz de Ballesteros, O. *Macromolecules* **2007**, *40*, 8531–8532. (d) De Rosa, C.; Ruiz de Ballesteros, O.; Auriemma, F.; Di Caprio, M. R. *Macromolecules* **2012**, *45*, 2749–2763. (e) Boragno, L.; Stagnaro, P.; Forlini, F.; Azzuri, F.; Alfonso, G. C. *Polymer* **2013**, *54*, 1656–1662.
- (7) Rieger, B.; Mu, X.; Mallin, D. T.; Rausch, M. D.; Chien, J. C. W. *Macromolecules* **1990**, *23*, 3559–3568.
- (8) This work has been presented in part at the symposium “Natta seeds grow: From the crystallography and modeling of stereoregular polymers to the challenges of complex systems” held at the Polytechnicum di Milano, Italy, 21–22 November 2013.
- (9) Cerius<sup>2</sup> User Manual; Accelrys: San Diego, CA, and Cambridge, UK.
- (10) (a) Klein, H.; David, J. *Acta Crystallogr.* **2011**, *A67*, 297–302. (b) Palatinus, L.; Jacob, D.; Cuville, P.; Klementová, M.; Sinkler, W.; Marks, L. D. *Acta Crystallogr.* **2013**, *A69*, 171–188.
- (11) Lovinger, A. J. *J. Polym. Sci., Polym. Phys. Ed.* **1983**, *21*, 97–110.
- (12) Lotz, B.; Graff, S.; Straupé, C.; Wittmann, J. C. *Polymer* **1991**, *32*, 2902–2910.
- (13) The accuracy of this value is slightly less than for the *a*- and *b*-axes parameters, due to the spread of the reflections along the *c*<sup>\*</sup> direction, which does not guarantee that the node of the reflection has been recorded.
- (14) Kusanagi, H.; Takase, M.; Chatani, Y.; Tadokoro, H. *J. Polym. Sci., Polym. Phys. Ed.* **1978**, *16*, 131–141.
- (15) Petraccone, V.; Pirozzi, B.; Frasci, A.; Corradini, P. *Eur. Polym. J.* **1976**, *12*, 323.

- (16) Petraccone, V.; Pirozzi, B.; Meille, S. V. *Polymer* **1986**, *27*, 1665–1668.
- (17) Sadler, D. M.; Spells, S. J.; Keller, A.; Guenet, J. M. *Polym. Commun.* **1984**, *25*, 290–293.
- (18) De Rosa, C.; Auriemma, F.; Ruiz de Ballesteros, O.; Resconi, L.; Camurati, I. *Macromolecules* **2007**, *40*, 6600–6616.
- (19) (a) Auriemma, F.; De Rosa, C.; Boscato, T.; Corradini, P. *Macromolecules* **2001**, *34*, 4815–4826. (b) De Rosa, C.; Auriemma, F.; Di Capua, A.; Resconi, L.; Guidotti, S.; Camurati, I.; Nifant'ev, I. E.; Laishevts, I. P. *J. Am. Chem. Soc.* **2004**, *126*, 17040–17049.
- (20) Turner-Jones, A.; Aizelwood, J. M.; Beckett, D. R. *Makromol. Chem.* **1964**, *75*, 134–158.
- (21) Rieger, B.; Lotz, B.; et al. Unpublished results.
- (22) VanderHart, D. L.; Alamo, R. G.; Nyden, M. R.; Kim, M. H.; Mandelkern, L. *Macromolecules* **2000**, *33*, 6078–6093.
- (23) Benedetti, E.; Pedone, C.; Allegra, G. *Macromolecules* **1970**, *3*, 16–19.
- (24) Tanaka, T.; Chatani, Y.; Tadokoro, H. *J. Polym. Sci., Polym. Phys. Ed.* **1974**, *12*, 515–531.
- (25) Wasai, G.; Saegusa, T.; Furukawa, J. *Makromol. Chem.* **1965**, *86*, 1–8.
- (26) Benedetti, E.; Pedone, C.; Allegra, G. *Macromolecules* **1970**, *3*, 727–735.
- (27) Ruan, JrJ.; Thierry, A.; Lotz, B. *Polymer* **2006**, *47*, 5478–5493.
- (28) Turner-Jones, A. *J. Polym. Sci., Polym. Lett.* **1963**, *1*, 455–456.
- (29) In the present analysis, the cell parameters determined by Turner-Jones have been used since they seem to have been accepted by the community, although they were given in a one-page letter, with no further structural determination or experimental support. A much later study (Petraccone et al. *Eur. Polym. J.* **1976**, *12*, 323–327) provides a “complete determination of this structure”. The reported cell dimensions are significantly larger:  $a = b = 15.42 \text{ \AA}$  and  $c = 21.05 \text{ \AA}$ , yielding a density of 0.819 only. This value is lower than the density of the amorphous phase and also lower than the reported density of the sample investigated.
- (30) Luciani, L.; Seppälä, J.; Löfgren, B. *Prog. Polym. Sci.* **1988**, *13*, 37–62.
- (31) Kopp, S.; Wittmann, J. C.; Lotz, B. *J. Mater. Sci.* **1994**, *29*, 6159–6166.
- (32) (a) De Rosa, C.; Auriemma, F. *J. Am. Chem. Soc.* **2006**, *128*, 11024–11025. (b) De Rosa, C.; Auriemma, F.; Perretta, C. *Macromolecules* **2004**, *37*, 6843–6855.
- (33) De Rosa, C.; Auriemma, F.; Ruiz de Ballesteros, O.; Esposito, F.; Laguzza, D.; Di Girolamo, R.; Resconi, L. *Macromolecules* **2009**, *42*, 8286–8297.